Sensors and Materials, Vol. 36, No. 7 (2024) 2983–3000
MYU Tokyo

S & M 3714

Mapping of Yangtze River Estuary Tidal Flat Based on Sentinel-2 Sensor and Google Earth Engine

Kuifeng Luan,[1,2] Haixia Wan,[1*] Zhenhua Wang,[3] Xuejun Lu,[4]
Zhuyuan Bei,[4] Jiansheng Yuan,[1,2] Zhaoxiang Cao,[1] Xinyi You,[1]
Jie Wang,[1,2] Wei Shen,[1,2] and Junfang Bi[5]

[1]College of Oceanography and Ecological Science, Shanghai Ocean University, Shanghai 201306, China
[2]Estuarine and Oceanographic Mapping Engineering Research Center of Shanghai, Shanghai 201306, China
[3]College of Information Technology, Shanghai Ocean University, Shanghai 201306, China
[4]Shanghai Marine Affairs Administration Center, Shanghai 200050, China
[5]Changjiang River Estuary Bureau of Hydrological and Water Resources Survey, Shanghai 200136, China

(Received March 15, 2024; accepted May 10, 2024)

Keywords: Otsu algorithm, maximum spectral index composite, tidal flat, Sentinel-2 sensor, Google Earth Engine

Delineating the distribution of tidal flats in the Yangtze River Delta region is of considerable significance for the ecological environment research and sustainable development of the region. However, the tidal flat ecology is greatly threatened by rapid economic development and human disturbance. Information on the tidal flat ecology is necessary for tidal flat extraction studies in Jiangsu Province and Shanghai City. Therefore, using imagery acquired by Sentinel-2 sensors along the coasts of Jiangsu Province and Shanghai City and the Google Earth Engine Cloud Platform, we established a multilayer automatic decision tree classification model based on the maximum spectral index composite algorithm and Otsu algorithm to extract tidal flats. A total of 1011 scene images, acquired from January 1 to December 31, 2021, were collected to generate tidal flat maps of Jiangsu Province and Shanghai City. The overall accuracy obtained by establishing the confusion matrix was 96.1%. The tidal flat areas of Jiangsu Province and Shanghai City in 2021 were 222347 and 41097 hectares, respectively, among which the tidal flat area of Jiangsu Province was 5.4 times that of Shanghai City. Moreover, we compared the results with real images and existing products, which further explained the rationality of the tidal flat results of this study. The 10-m-resolution tidal flat map of Jiangsu Province and Shanghai City obtained in this study can provide support for the sustainable policy management of tidal flats in the Yangtze River Delta region.

1. Introduction

Tidal flats are transitional zones between marine and terrestrial environments. They are sensitive areas where the two environments intersect and include mud, sand, and rocky flats in intertidal zones. They allow global ecosystem services, including climate regulation, carbon

*Corresponding author: e-mail: m210200598@st.shou.edu.cn
https://doi.org/10.18494/SAM5047

ISSN 0914-4935

sequestration, and shoreline maintenance.[1] In addition, they provide habitats for many marine and terrestrial organisms, maintain biodiversity, and are essential for maintaining the ecological balance in the region.[2] However, as an important ecosystem, tidal flats are very fragile[3,4] and are seriously threatened by human activities and natural changes.[4] For example, the rapid expansion of aquaculture on a global scale has led to the alteration of large areas of valuable coastal land, which has had a strong negative impact on natural ecosystems, including the destruction of coastal wetlands, the loss of biodiversity, and the pollution of water and soil.[5,6] More changes, such as the destruction of tidal flats by artificial seawalls and tidal flat erosion due to sea level rise, lead to the loss of many tidal flats and intertidal habitats, affecting tidal flat biodiversity.[7] According to the International Union for the Conservation of Nature (IUCN), the loss of intertidal habitats is a major threat to many countries.[8] With human development and climate change, the loss of intertidal habitat has become so complete and sudden that birds have little time to adapt. Therefore, it is necessary to map tidal flats with high resolution and accuracy.

Tidal flats are an important part of the coastal ecosystem in Jiangsu Province and Shanghai City and are under significant threat.[9,10] Shanghai City, a super-large city in China, has a GDP of 4465.28 billion yuan. Economic development and environmental issues in this region have received considerable attention. In particular, the ecological environment and a vast majority of coastlines have suffered extensive damage due to economic development. For example, in Shanghai City, reclamation projects are being implemented to expand urban land areas and support economic development,[11] which usually involve the reclamation of land from the sea, i.e., turning the original sea into land.[12] In particular, large-scale reclamation projects in the Yangtze River Estuary area include Donghengsha and Pudong coastal reclamation, which may cause the original tidal flats to be submerged or destroyed.[1,13] Reclamation projects alter marine ecosystems in coastal areas, adversely affecting ecological elements, such as fish, benthos, and birds.[14] Jiangsu Province ranks second in terms of GDP among 31 provincial administrative regions in mainland China, and the economic benefits of coastal aquaculture ponds are clear[15] China is the world's largest producer of aquaculture, accounting for approximately 61.5% of the global production. Jiangsu Province has large-scale aquaculture ponds, which are mainly used for aquaculture products such as shrimp, crab, and fish.[5] However, the expansion of coastal aquaculture ponds also poses severe environmental problems. The construction of aquaculture ponds usually requires the occupation of coastal wetlands and tidal flats because of the saline-alkali soils in these areas, which are conducive to aquaculture. This may result in the reduction or alteration of tidal flats, as existing wetlands and tidal flats are used to build ponds.[16] Additionally, pollutants may be introduced during farming, posing a potential threat to tidal flats and the surrounding ecosystems.[16] The governments of Shanghai City and Jiangsu Province make extensive efforts to effectively manage the deteriorating tidal flat ecosystem and achieve the sustainable development of the coastal resources of China. Therefore, the study of up-to-date and reliable tidal flat maps in Shanghai City and Jiangsu Province is critical to maintaining ecological balance, disaster prevention, and the economy.

For the monitoring and mapping of tidal flats, field investigations are difficult owing to periodic variations in tides. The mapping of tidal flats in small areas relies mainly on field measurements, such as unmanned aerial vehicle and bathymetric lidar measurements; however,

owing to data availability, openness, and price, it is not feasible to apply these methods to large-scale tidal flat mapping.[17] Remote sensing technology has the advantages of high effectiveness, a large amount of information, and multiple platforms. Its rapid development provides a new method for identifying tidal flats and plays an increasingly important role in tidal flat identification.[18,19]

In recent years, numerous studies have used satellite remote sensing images to extract tidal flat information at the local, national, and global scales. Currently, three main methods are used for tidal flat mapping based on remote sensing images: tidal models, machine learning based on training samples, and decision trees based on prior knowledge.[18,20,21] In the first method, which is based on tidal models or topography, satellite remote sensing data are used to capture the position of the coastline at different times. The predicted data of tidal models are then combined to monitor water level changes under different tidal conditions and determine the contour and extent of tidal flats. For example, Murray *et al.*[22] used regional tidal models to acquire remote sensing images of high and low tides, determined instantaneous water boundaries, and mapped intertidal wetlands along the coast of East Asia. Sagar *et al.*[20] mapped tidal flats in Australia using a continental-scale tidal model combined with the median pixel synthesis of normalized difference water index (NDWI) stacks using full-time-series Landsat observations. However, owing to the scarcity of intertidal elevation, the complexity of coastal topography, and the spatial variation of tidal levels, the application of this method to large areas causes great uncertainty. The second method is a machine learning method based on training samples and uses remote sensing image data with label information to create a machine learning model that automatically identifies and labels tidal flat areas to achieve tidal flat mapping. Zhang *et al.*[23] mapped coastal tidal flats in eastern China using machine learning classification methods based on the Google Earth Engine (GEE) platform. On the basis of the GEE platform, Murray *et al.*[18] analyzed more than 700000 Landsat satellite images globally to map the extent of and changes in tidal flats from 1984 to 2016. They found that approximately 70% of the global tidal flats were distributed in Asia, North America, and South America, and 16.02% of the global tidal flats disappeared in 33 years. However, these classifications rely on a large number of training samples and are often time-consuming and labor-intensive. The third method is the knowledge-based decision tree method, which is based on expert knowledge and rules and gradually delineates the tidal flats in the images through a decision tree. For example, Wang *et al.*[21] mapped tidal flats in China using a decision tree algorithm based on prior knowledge from Landsat data and the GEE platform. These studies extracted tidal flats using empirical knowledge and statistical data derived from universal thresholds. However, because of the complexity of tidal flats in different areas, universal thresholds may not apply to large areas. Current tidal flat research methods lack robust, accurate, and universal classification methods for simultaneously mapping tidal flats. Classification approaches should not be dependent on pre-existing information such as tidal levels on the dates of image capture, significant phenological dates, artificially outlined shoreline data, or experiential thresholds.

Recently, Earth observation satellites have become the primary data source for large-scale coastal land cover mapping. Time-series Sentinel-2 Sensor acquired images and GEE platforms have great potential for mapping tidal flats with detailed spatial information.[14,19,21]. Sentinel-2

Sensor acquired images have revisit intervals of 2–5 days, and the high temporal resolution provides an excellent opportunity to capture the lowest and highest tides, which is critical to accurately determine the extent of tidal flats. However, satellite images have several shortcomings when mapping tidal flats. Because of the wide coverage of a single satellite image, there are continuous tidal changes in the region, and accurately obtaining low tide and high tide images in different regions is difficult. In addition, owing to the possible cloud occlusion, tidal images that have been obscured by clouds for a long time cannot be effectively filtered out. The GEE has a strong potential for remote sensing analysis and is widely used in coastal zone research. The GEE is a cloud-based analytics platform that includes a large amount of publicly available geospatial data, analytically available Landsat data, and high-performance parallel computing services. Many scientists have conducted various studies related to land cover mapping on the GEE platform. For example, Li *et al.*[14] constructed a Sentinel-2 normalized difference vegetation index (NDVI) time series from January 2017 to December 31, 2018, characterized the changing track of mangrove phenological characteristics, and verified the feasibility of the random forest algorithm on the basis of phenological characteristics to classify mangrove species on the GEE platform. Xu *et al.*[24] put forth a straightforward phenological vegetation index (PVI) that relies on the pixel-wise composition of Sentinel-2 observational data, utilizing the GEE platform. They confirmed the applicability of the random forest algorithm for classifying mangrove species and found that the supervised Otsu-PNDVI technique exhibits high accuracy in classifying *Spartina alterniflora*.

Although several local-scale studies were conducted, the latest high-resolution tidal flat conditions in Jiangsu Province and Shanghai City remain unclear. In this study, we aimed to realize the automatic and high-precision extraction of intertidal wetlands in Jiangsu Province and Shanghai City using Sentinel-2 Sensor acquired images and GEE cloud platforms. To address the above-mentioned issues, in this study, we include (1) fast and automatic tidal flat mapping using Sentinel-2 Sensor acquired time series images and the GEE platform, (2) comprehensive verification using tidal station measurement data, existing research data, and selected edge points to evaluate the accuracy of tidal flat mapping results in Shanghai City and Jiangsu Province, and (3) the analysis of possible reasons for the spatial variation of tidal flats in Jiangsu Province and Shanghai City .

2. Data, Materials, and Methods

2.1 Study areas

The study areas were Shanghai City and Jiangsu Province, China (Fig. 1). Shanghai City is located at 120° 52′–122° 12′ E and 30° 40′–31° 53′ N, with a land area of 6340 km^2. This place is situated on the western shore of the Pacific Ocean and at the eastern boundary of the Asian landmass, and serves as the meeting point of China's northern and southern coastlines. It is positioned where the Yangtze River and Huangpu River merge into the sea. Its geographical boundaries are the Yangtze River to the north, the East China Sea to the east, Hangzhou Bay to the south, and the provinces of Jiangsu Province and Zhejiang to the west. Because of the special geological and geomorphological environment and water and sediment conditions in the Yangtze

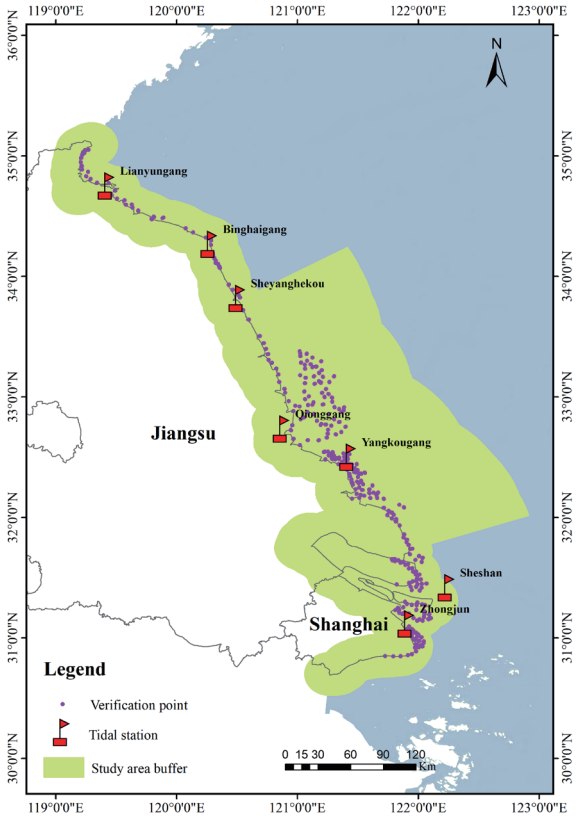

Fig. 1. (Color online) Map of study area (Jiangsu Province and Shanghai City) showing the positions of edge validation points. A total of 624 samples were randomly selected along the coast.

River Estuary and Hangzhou Bay, the tidal flats in the Shanghai City area have a unique distribution and ecological environment. Shanghai City tidal flats are mainly distributed in the east and south of Shanghai City and in the coastal zone near the Yangtze River estuary.[25] Jiangsu Province, which spans 30° 45'–35° 08' E, 116° 21'–121° 56' N, belongs to the East Asian monsoon climate zone and is located in the subtropical and warm temperate climate transition zone, where the annual precipitation is 704–1250 mm. The tidal flats in Jiangsu Province are mainly distributed along the coastlines of the Yellow Sea and East China Sea, as well as in the estuary near the Yangtze River estuary. Jiangsu Province has the largest tidal flat wetland in China,[9] which is the habitat of many birds, shellfish, and other organisms with rich species diversity.[21]

2.2 Dataset

2.2.1 Sentinel-2 Sensor data

Sentinel-2 Earth observation satellites were launched by the European Space Agency (ESA) for remote sensing and environmental monitoring missions. Sentinel-2 consists of two polar-orbiting satellites (Sentinel-2A launched in June 2015 and Sentinel-2B launched in March 2017),

with a revisiting period of 10 days for individual satellites and 3–5 days for the combined constellation. Sentinel-2A represents a novel high-resolution multispectral imaging satellite, predominantly employed for worldwide land observations, which includes the monitoring of land vegetation, soil, and water resources, inland water bodies, coastal regions, and services related to emergency rescue.[26] The satellite image data acquisition time was from January 1, 2021 to December 31, 2021, covering the entire area of Shanghai City and Jiangsu Province, and 1011 images were acquired.

In this study, we applied the Sentinel-2 sensor data L2A product, which contains surface reflectance data after atmospheric correction. Images with greater than 50% cloud cover were filtered out, and pixels with low observation quality, such as opaque clouds, cirrus clouds, and shadows in each image, were masked by the QA60 band.[27] The remaining pixels were retained as high-quality observation data. Taking into account computational efficiency and the presence of one of China's most extensive tidal flats in southern Jiangsu Province, the research area was further narrowed down to a buffer zone extending 20 km from the northern Jiangsu Province coastline and 100 km from the southern Jiangsu Province coastline. A total of 1011 images covering the entire coastal areas of Shanghai City and Jiangsu Province were used for further analysis.

2.2.2 Verification samples

For evaluating the accuracy of the produced tidal flat map, a total of 624 samples were chosen randomly from the coastal area of the study region. The geographical arrangement of these sample points is depicted in Fig. 1. All these samples were sourced from high-resolution images on Google Earth or from Sentinel-2 Sensor acquired images taken at low tide. By visual interpretation, samples were labeled into two categories: tidal flat and others. Thus, the overall, user, and producer accuracies for each category were derived from the confusion matrix.[9,19]

In this study, we randomly identified completely exposed tidal flat points and their edge points, and established verification points as key references to verify the accuracy of tidal flat maps for Shanghai City and Jiangsu Province. To identify the edge points, we chose seven crucial tidal stations, located from the northern to southern parts of the coast. Daily time-by-time tide data for these stations are available at the National Oceanographic Science Data Center (https://mds.nmdis.org.cn/pages/tidalCurrent.html). On the basis of Sentinel-2 satellite transit times and tide tables, daily tide data were matched to seven images acquired at local low tide, showing that the tidal flats were fully exposed. Information on these images and instantaneous tide heights is summarized in Table 1. For the selection of edge verification points, the Qionggang Station in Jiangsu Province was used as an example. The largest tidal flat in China is located near the Qionggang Station. By screening the high-quality Sentinel-2 image corresponding to the lowest tide level at the transit time [Fig. 2(A)], the transit date of the lowest tide image was determined, and the tide level height at the transit time of the image was obtained from the tide table of that day [Fig. 2(B)]. From the Sentinel-2 image captured during peak tide [Fig. 2(C)], we randomly picked pixels representing both pure tidal and nontidal flats along the periphery of the tidal flat patch to serve as edge points [Fig. 2(C)–(E)]. Thus, we acquired 624

Table 1
General characteristics of tidal stations (from north to south), time of image acquisition, and temporal tidal status.

Province	Station name	Sentinel-2 Sensor transit time	Instantaneous tide height (cm)	Tide status
Jiangsu	Qionggang	01-18-2021 10:40:29	87	Local lowest
	Binghaigang	03-24-2021 10:44:16	66	Local lowest
	Yangkougang	07-17-2021 10:47:28	196	Local lowest
	Lianyungang	12-02-2021 10:50:52	99	Local lowest
	Sheyanghekou	12-07-2021 10:45:52	142	Local lowest
Shanghai	Zhongjun	02-04-2021 10:29:07	79	Local lowest
	Sheshan	02-04-2021 10:29:07	30	Local lowest

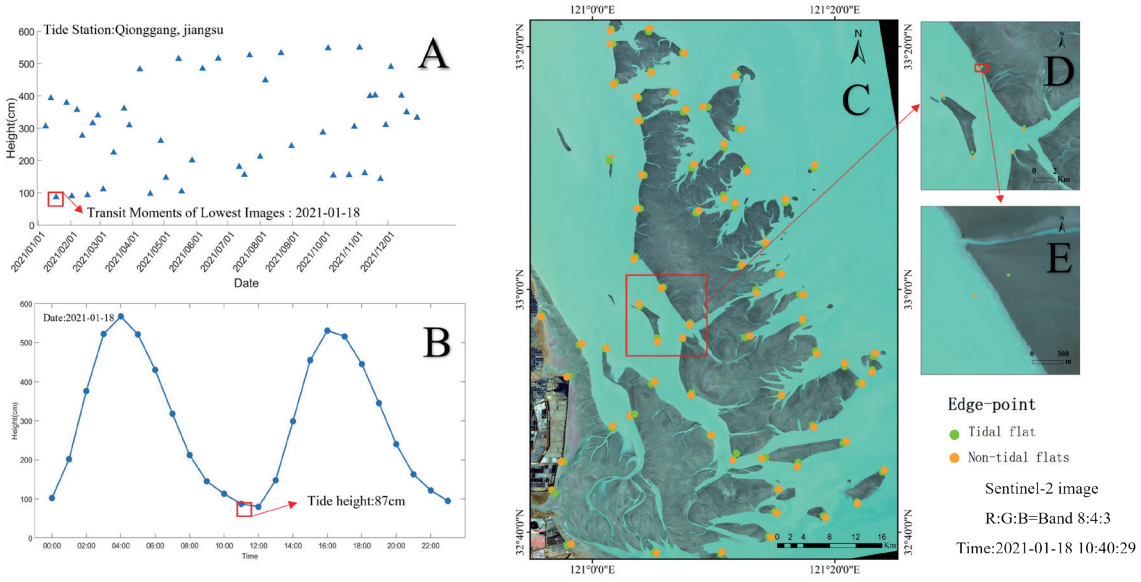

Fig. 2. (Color online) Edge point selection near Qionggang Station. (A) Transit lowest tide date of January 18, 2021 for Qionggang Station image. (B) Tide table for Qionggang Station on January 18, 2021. The minimum tide image transit time is 11:00:00 a.m., and the tide height is 87 cm. (C) Lowest tide image captured by Sentinel-2 Sensor at 10:40:29 a.m. (C–E) Edge point location.

edge validation points, which were distributed from the northern to southern parts of the area. Pure tidal and nontidal flat edge points can reflect whether our synthetic map contains completely exposed tidal flat patches and can be used to test whether the pixels of high-turbidity river water and building land are misclassified as tidal flats. The sampling method of randomly selecting the pixels at the edges of the tidal flat patches provides a more accurate verification for extracting the shape features of the tidal flat edges. Therefore, edge point verification is key to verifying the accuracy of the obtained tidal flat map.

2.3 Method

In this study, we developed an automatic, fast, and high-precision tidal flat extraction method based on the maximum spectral index composite (MSIC) algorithm and Otsu method, which mainly included the following steps: (1) the construction of a high-quality dense time-series Sentinel-2 Sensor acquired image stack based on the GEE cloud platform, (2) the selection of a suitable spectral index according to the time-series variation characteristics of tidal flats and the synthesis of maximum and minimum water surface images from a high-quality time-series data set based on the MSIC algorithm, (3) the construction of a multilayer decision tree automatic classification model based on the Otsu algorithm to extract beach area, and (4) the noise removal and verification of quantitative visualization for beach area.[9,28] The workflow is illustrated in Fig. 3.

2.3.1 Image synthesis method based on MSIC

After the removal of cloud cover, the modified normalized difference water index (mNDWI)[29] and NDVI[30] of each pixel in the image collection were calculated. Table 2 shows both the indices. All preprocessing tasks for building collections were performed in the GEE platform. The mNDWI is widely used to distinguish open surface water from other features

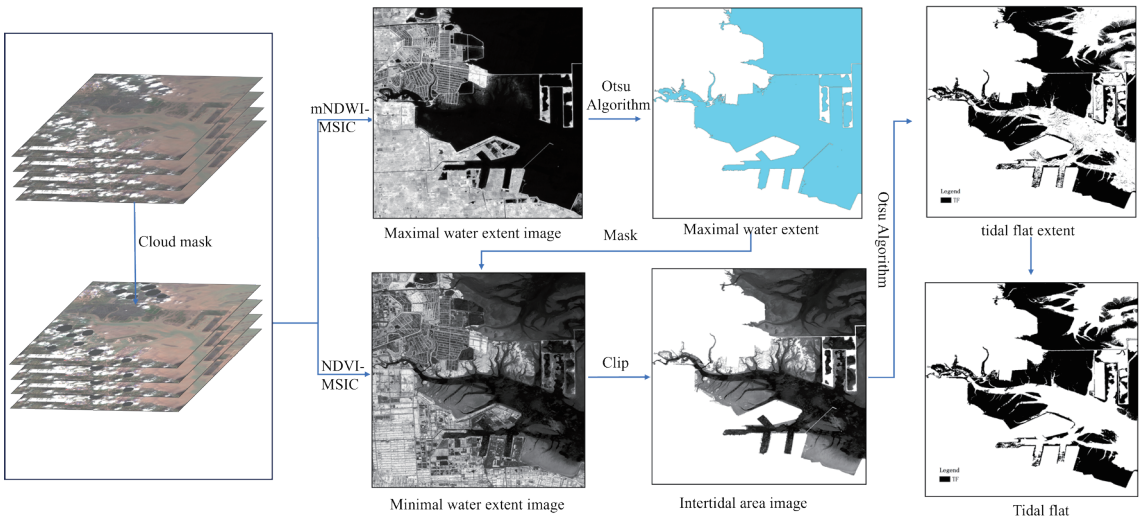

Fig. 3. (Color online) Workflow of tidal flat mapping in this study. TF: tidal flats.

Table 2
Spectral index equations used in this study.

Name	Abbreviation	Equation
Nominalized difference vegetation index	NDVI	$(\rho_{nir} - \rho_{red})/(\rho_{nir} + \rho_{red})$
Modified normalized difference water index	mNDWI	$(\rho_{green} - \rho_{swir})/(\rho_{green} + \rho_{swir})$

Here, ρ_{nir} is the reflectance of the near-infrared band (Band 8 of Sentinel-2 Sensor acquired images), ρ_{red} is the reflectance of the red band (Band 4 of Sentinel-2 Sensor acquired images), ρ_{green} is the reflectance of the green band (Band 3 of Sentinel-2 Sensor acquired images), and ρ_{swir} is the reflectance of a short-wave infrared band (Band 11 of Sentinel-2 Sensor acquired images).

using different sensors (such as Landsat). It enhances the difference between artificial shorelines and water bodies, such as levees (roads and pond edges), and effectively suppresses the effects of other background water bodies, such as aquaculture ponds.[31] The NDVI is used to obtain the lowest tide image, which can significantly increase the difference between vegetation, beach, and water and can effectively avoid the interference of tidal uncertainty on beach extraction.

GEE API provides "imageCollection.qualityMosaic()", MSIC selects a quality band as a pixel-by-pixel sorting function to extract the data with the maximum value after the superposition and sorting of the specified bands of the pixel, which is used as the source of each pixel in the final synthesized image. The details can be found at https://developers.google.com/earth-engine/guides/ic_composite_mosaic.

Within a full tidal cycle, a pixel of a tidal flat can be recognized as either a tidal flat or a water body, due to tidal variations. The mNDWI extremum synthesis technique was utilized on a stack of Sentinel-2 Sensor acquired images to determine the effects of these tidal changes. The extreme values encompass both the highest and lowest points. In the image stack, the mNDWI at a pixel location varied with the tidal cycles, with higher and lower mNDWIs corresponding to water and land, respectively. The mNDWI maximum composite image (mNDWI-MSIC) can be used to extract areas where seawater historically exists in tidal flats or other characteristic areas; therefore, the largest mNDWI-MSIC represents the largest water area.[9,23] In contrast, if the location is exposed to the sea surface, the highest NDVI can be recorded because the NDVI of water is lower than those of the other features. Thus, the largest NDVI-MSIC depicts the smallest water area.[9]

2.3.2 Water–land separation based on Otsu algorithm

By selecting an appropriate threshold, objects in a synthetic image can be segmented into two classes. The Otsu algorithm, proposed by Otsu in 1979, is a nonparametric method for selecting the optimal threshold based on the image's statistical attributes. It functions as an automatic classification model resembling a multilayer decision tree.[32,33] According to the gray characteristics of the image, the image is divided into background and foreground on the basis of the principle by the least squares method. The basic logic of the algorithm is to select the value with the largest variance between classes and the smallest variance within classes as the optimal threshold for automatically classifying the image. Equation (1) is as follows:

$$t^* = \arg\max_{1\le t\le n}\left\{ w_0(t)\, w_1(t)\left[m_1(t) - m_2(t)\right]^2 \right\}, \tag{1}$$

where t^* is an arbitrary threshold, representing the optimal threshold, n represents the gray level of the pixel, $w_0(t)$ and $w_1(t)$ represent the possibilities of two classes appearing at pixel level t, $m_1(t)$ and $m_2(t)$ represent the mean values of two classes at pixel level t, and the image is synthesized by traversing extreme values. When $w_0(t)w_1(t)[m_1(t) - m_2(t)]^2$ (interclass variance) is maximum, the corresponding t value is selected as the optimal threshold for segmentation. The tidal flat was identified by obtaining the synthetic images of the maximum and minimum water areas of the study area, applying the Otsu method and selecting the optimal threshold.

2.3.3 Denoising and accuracy assessment

From the obtained preliminary tidal flat map, pixel groups smaller than 100 units were eliminated by using the "connetedPixelCount" function in GEE to remove small nontidal flat noise points. A large amount of noise was removed in this process.

The confusion matrix was calculated on the basis of samples from the classified tidal flats and other categories using three metrics: producer accuracy (PA), user accuracy (UA), and overall accuracy (OA).[9,19,34] PA represents the probability of a land cover map accurately classifying a ground feature class, thereby assessing the omission error. UA evaluates the consistency between the tidal wetland categories in satellite-derived maps and the reference data, and assesses commission errors. OA is the ratio of the number of pixels correctly classified to the total number of pixels, serving as a metric for evaluating the classification outcomes and data agreement.

3. Results

3.1 Accuracy assessment of tidal flat classification

The accuracy of the 10-m-resolution tidal flat maps generated for Shanghai City and Jiangsu Province for 2021 was verified. The results showed that the tidal flats were accurately mapped, with accuracy rates of more than 95% for both UA and PA and OA rates as high as 96.1% (Table 3). From a regional perspective, the OA of Jiangsu Province was 96.4%, which was higher than that of Shanghai City (95.3%). This is because the turbid water in Shanghai City might have affected the identification of tidal flats using the algorithm, which is consistent with the results of Jia *et al.*[9]

3.2 Spatial distribution characteristics of tidal flat

Figure 4 shows the spatial distribution of tidal flats along the coastlines of Shanghai City and Jiangsu Province extracted by the MSIC-Otsu method. The total area of tidal flats in Shanghai City and Jiangsu Province is 263444.0 hectares. Jiangsu Province is larger than Shanghai City, and its tidal flat area is 5.4 times that of Shanghai City.

Table 3
Confusion matrix for each map.

Region	Class	TF	Non-TF	UA	OA
Shanghai	TF	84	6	93.3%	95.3%
	Non-TF	2	80	97.5%	
	Pro. acc.	97.6%	93.0%		
Jiangsu	TF	215	5	97.7%	96.4%
	Non-TF	11	221	95.2%	
	Pro. acc.	95.1%	97.7%		
Total	TF	299	11	96.4%	96.1%
	Non-TF	13	301	95.8%	
	Pro. acc.	95.8%	96.4%		

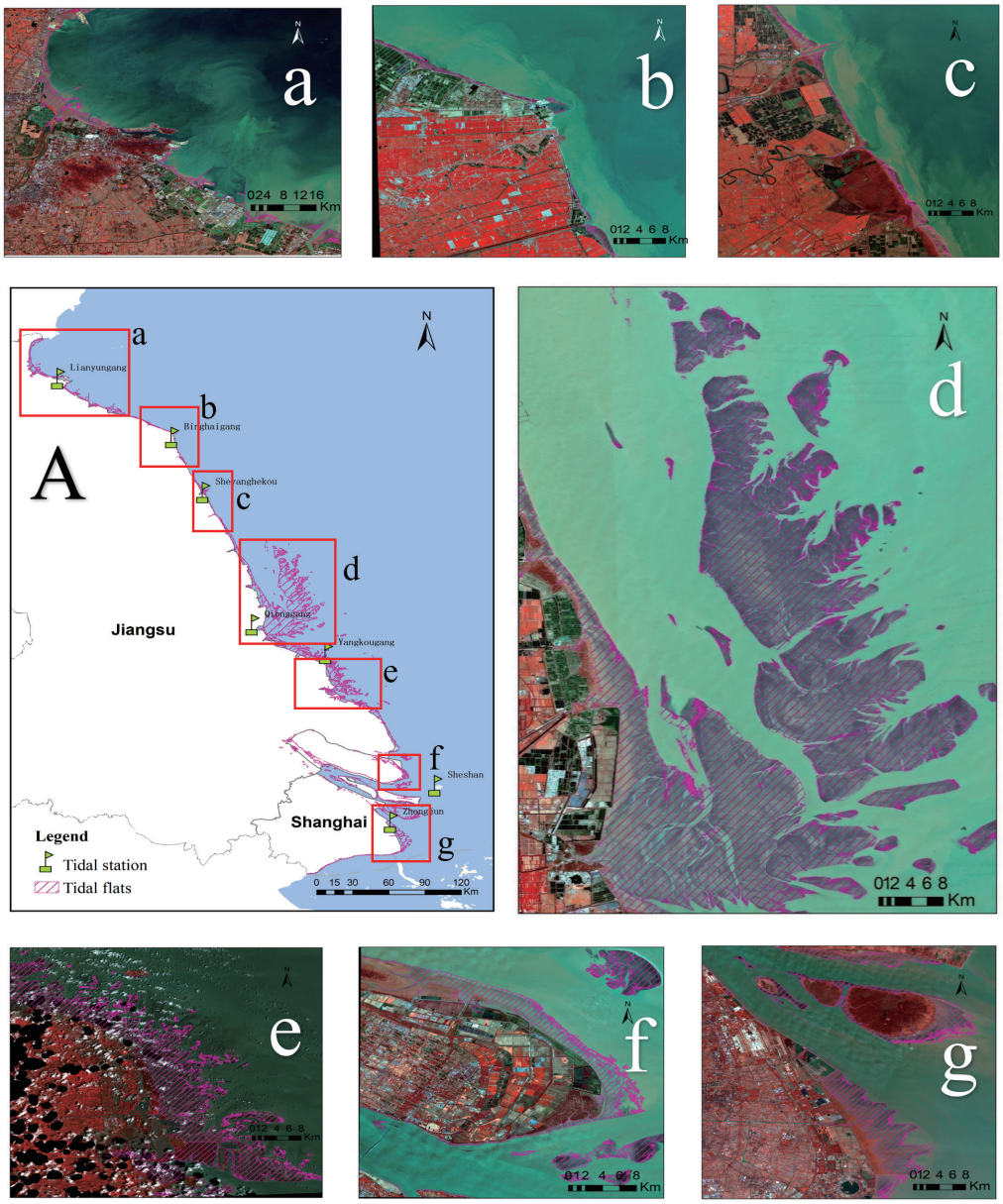

Fig. 4. (Color online) Beach distribution in Jiangsu Province and Shanghai City. (a) Linhong Estuary, (b) abandoned Yellow River Estuary, (c) Sheyang Estuary, (d) Liangduo Estuary, (e) Lusigang, (f) Chongming Island, and (g) Nanhui Xincheng Beach. The purple line in subfigures (a)–(g) delineates the extent of tidal flats proposed by our method. The optical base maps used in subfigures (a)–(g) are the false-color Sentinel-2 images obtained during the lowest tide, at 10:50:52 on 2 December 2021, 10:44:16 on 24 March 2021, 10:45:52 on 7 December 2021, 10:40:29 on 18 January 2021, 10:47:28 on 17 July 2021, 10:29:07 on 4 February 2021, and 10:29:07 on 4 February 2021, respectively.

To show the details of the tidal flat map more visually, the tidal flat maps of Jiangsu Province and Shanghai City were divided into seven subregions from north to south: the Linhong Estuary [Fig. 4(a)], abandoned Yellow River Estuary [Fig. 4(b)], Sheyang Estuary [Fig. 4(c)], Liangduo

Estuary [Fig. 4(d)], Lusigang [Fig. 4(e)], Chongming Island [Fig. 4(f)], and Nanhui Xincheng Beach [Fig. 4(g)]. The tidal flat distribution that we obtained was superimposed on the real low tide image for display, in which the low tide image was combined with the tide height data from the tide station to find the image corresponding to the lowest tide level at the moment of image transit, the details of which are shown in Table 1. Overall, the tidal flat classification was accurate, and the tidal flat area was clearly divided. Large tidal flats are mainly distributed in estuaries and deltas with large tidal differences and high sediment inflow, such as the Liangduo Estuary [Fig. 4(d)], Lusihe Estuary [Fig. 4(e)], and Nanhui Xincheng Beach [Fig. 4(g)]. For example, in the estuary of the Yangtze River, the longest river in Asia, a distinct tidal flat forms in Shanghai City [Fig. 4(g)]. The Liangduo Estuary [Fig. 4(d)] in the Yancheng area is continuously supplied with sediment because of the southward coastal current and circular currents of the abandoned Yellow River Estuary, which is in a siltation environment and rich in tidal flat resources. We found that the mapped contours of the tidal flat were in good agreement with the satellite images.

4. Discussion

4.1 Reliability of edge extraction at high and low tides

Observation frequency plays an important role in mapping tidal flats. Even though the Sentinel-2 Sensor has a repetition period of two days, only a portion of the tidal flats is inevitably captured at a given time. Because of the effects of ground albedo and clouds, remote sensing images are often incomplete, and a single image cannot show the characteristics of large areas. Additionally, tidal variations within a scene can introduce uncertainty into tidal flat mapping. In earlier studies, high and low tides were determined on the basis of the artificial selection of high and low tide images[35] or on the assumption that percentiles were the lowest and highest tide data.[36] Manually determining images of high and low tides can be time-consuming when dealing with extensive regions. In addition, the percentile selection method may lead to the inclusion of the lowest and highest tides in the lower and upper quantiles, respectively. The cartographic work in this study was based on the assumption that images were obtained near the lowest and highest tides. Instead of choosing the images of the highest and lowest tides from the observed scene, we utilized the MSIC method, which amalgamates the images of the highest and lowest tides.[9,19] MSIC is an automatic technique that requires no human input, training sets, or supplementary data during the mapping procedure. It also does not require any extra masking, preprocessing, or postprocessing stages to alter the initial mapping outcomes.[9]

Next, the reliability of the results of extracting the maximum and minimum tidal lines is discussed by combining data from tidal stations and images. The highest tide date was selected when the satellite passed through the tide data of one year, and then the tide height was obtained at the image transit time using the tide table of that day, which was downloaded as a satellite image. Similarly, the time points of the second high tide, second low tide, and lowest tide were selected on the basis of the tide height data at the image transit time, and the corresponding satellite image data was downloaded. Additionally, the maximum water area image obtained from the mNDWI-MSIC maximum synthesis map was used as the generated high-water line,

and the minimum water area image obtained from the NDVI-MSIC maximum synthesis map was used as the generated low-water line.

As shown in Fig. 5, considering the tidal flat near Yangkou Port in Jiangsu Province as an example, we displayed the true-color Sentinel-2 Sensor acquired image of the highest, intermediate, and lowest tides superimposed on the high- and low-tide lines extracted in this study. In the image of the highest tide at 728 cm [Fig. 5(a)], the tidal flat completely disappeared, and only the town was observed. The outline boundary of the enclosed artificial island and that of the Yellow Sea Bridge connecting Sunshine Island and inland land in the figure are consistent with the water–land boundary line of the high-tide image. The extracted high-tide line coincided

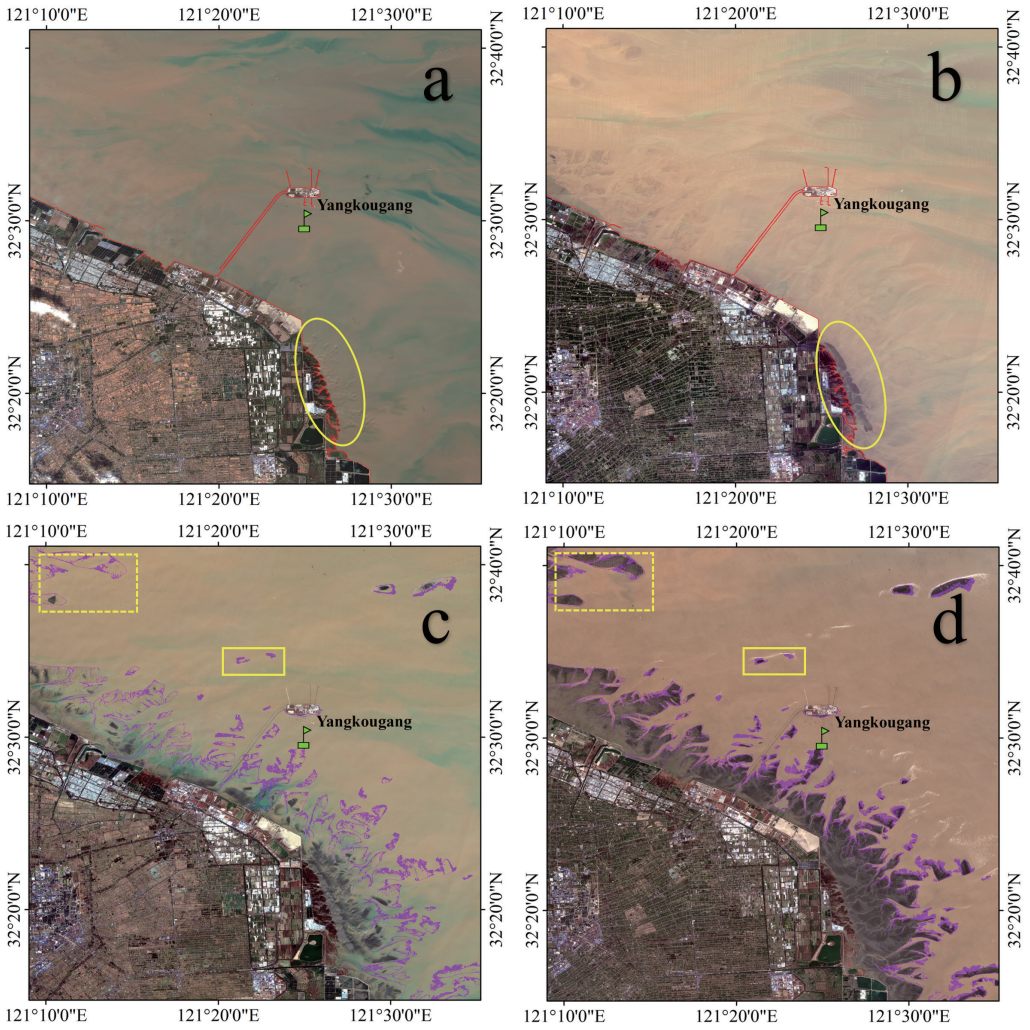

Fig. 5. (Color online) Selection of the tidal flat near Yangkou Port, Jiangsu Province, China. (a) Highest tide Sentinel-2 Sensor acquired image taken at 10:38 a.m. on November 4, 2021, and the tidal flat corresponding to 11:00 a.m. was 728 cm, (b) Sentinel-2 Sensor acquired image taken at 10:47 a.m. on March 29, 2021, and the tidal flat corresponding to 11:00 a.m. was 586 cm, (c) Sentinel-2 Sensor acquired image taken at 10:47 a.m. on December 29, 2021, and the tidal flat corresponding to 11:00 a.m. was 386 cm, and (d) lowest tide Sentinel-2 Sensor acquired image taken at 10:37 a.m. on February 17, 2021, and the tidal flat corresponding to 11:00 a.m. was 252 cm.

with the water–land boundary line corresponding to the high-tide image. In the tide image at the middle tide level of 586 cm [Fig. 5(b)], exposed tidal flats were found southeast of the town, and the extracted high-tide line was located inside the exposed tidal flats [Fig. 5(b), yellow ellipse]. When the tide level was lower than the highest tide level, the image change between the artificially constructed shoreline area and the highest tide period was clear, whereas that between the tidal flats in the southeastern direction of the town without artificial intervention and the highest tide period was unclear [Fig. 5(b), yellow ellipse]. This indicates that different tidal levels have larger water-edge extraction results, showing the impact of human activities on tidal flats. At the lowest tide time, the tide level was 252 cm on the image [Fig. 5(d)]; the purple line is the low-tide boundary line extracted using the proposed method. It was found that all the tidal flats were identified, and the extracted low-tide line was consistent with the corresponding tidal flat outer edge line in the lowest tide image. Compared with Fig. 5(d), Fig. 5(c) shows the sub-low tide (386 cm tide level). The submerged tidal flats far away from the shoreline [yellow solid line and dotted rectangle in Fig. 5(c)] and smaller tidal flat areas near the town indicate that the extraction difference of tidal flats was large at different tide levels, highlighting the irrationality of setting the percentile for tidal flat extraction.

4.2 Comparison with other studies

We compared our tidal flat results in area and space with those of other studies: tidal flat map 2018 (hereafter referred to as Wang_TF),[21] tidal flat map January 2019–June 2020 (hereafter referred to as Jia_TF),[9] tidal flat map 2014–2016 (hereafter referred to as Murray_TF),[18] and tidal flat map 2020 (hereafter referred to as Zhang_TF).[34]

First, we observed some differences between the datasets, as shown in Fig. 6. Our Jiangsu Province tidal flat area was larger than those of Wang_TF and Jia_TF and smaller than those of Murray_TF and Zhang_TF. The Shanghai City tidal flat area was larger than those of Wang_TF,

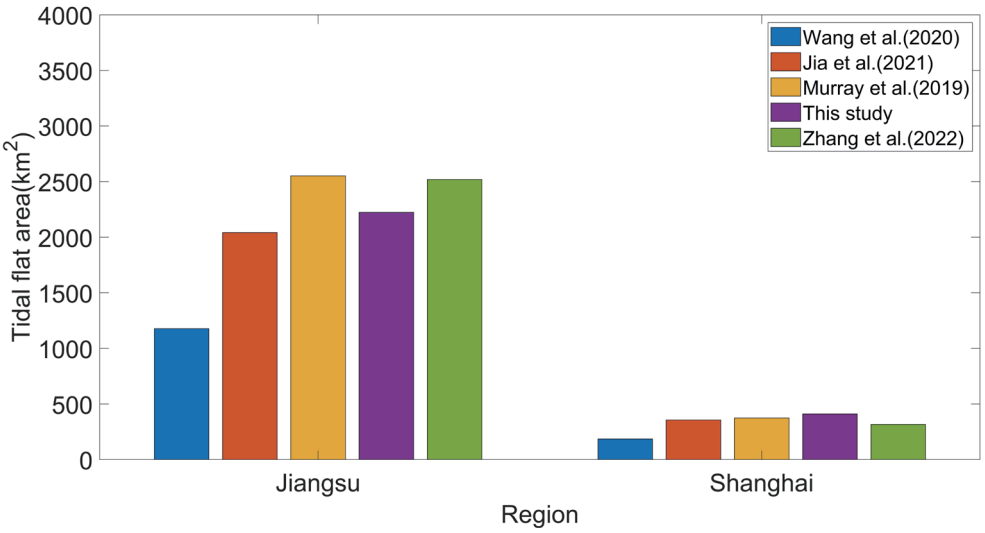

Fig. 6. (Color online) Bar plot comparing the tidal flat areas of Jiangsu Province and Shanghai City with those of Wang_TF,[21] Jia_TF,[9] Murray_TF,[18] and Zhang_TF.[34]

Jia_TF, Murray_TF, and Zhang_TF. Wang_TF, Murray_TF, and Zhang_TF used the Landsat data. The revisit period of the Landsat data is 16 days; therefore, it cannot capture high and low tides completely. Furthermore, a resolution of 30 m leads to wider bands; therefore, it cannot provide finer tidal flat results than sentinel sensor data. The low tidal flat area of Wang_TF is also related to the division of most tidal flats into water areas. Temporal variations and tidal flat definitions also cause areal differences. For example, in the definition of tidal flats, Jia_TF defines the vegetation-free sediment area between the high- and low-tide lines as tidal flats. In terms of time variation, the results for Murray_TF were the tidal flats from 2014 to 2016.

As shown in Fig. 7, the tidal flat results of this study differ significantly from those of Murray_TF, which may not be solely due to the data source and tidal flat evolution. Combining the tidal flat distribution map of Murray_TF and the algorithm details, it can be seen that in the tidal flat result identification of Murray_TF, the sediment and culture pond on the beach are regarded as tidal flat identification, which is the most important reason for the difference between our results and that of Murray_TF. As Murray *et al.*[18] and Zhang *et al.*[34] did not consider the effect of low tide, they did not capture many low-tide beaches.

Our interpretation of tidal flats is consistent with that of Zhang_TF. However, Zhang_TF employs the random forest technique. In this technique, certain mudflats or sandy beaches situated above the high-tide line are categorized as tidal flats, but they are not classified as tidal

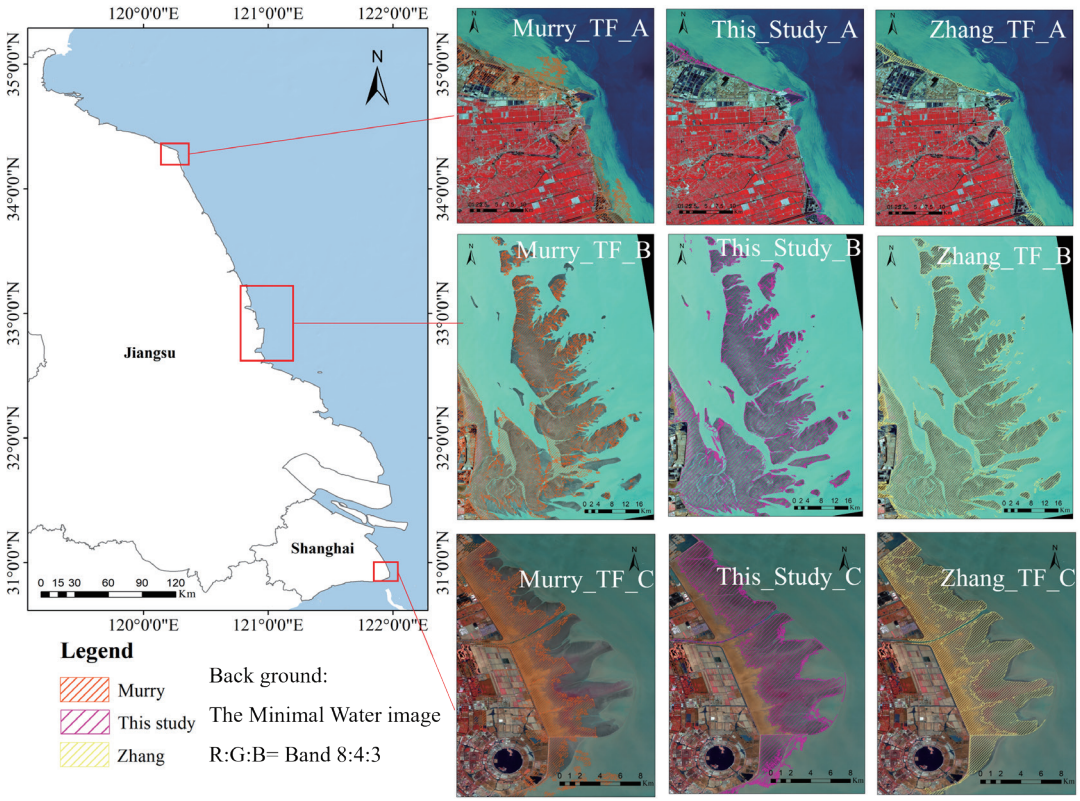

Fig. 7. (Color online) Subset views of tidal flats in Murray_TF,[18] this study, and Zhang_TF[34] located in the abandoned Yellow River Estuary (Area A), Liangduo River Estuary (Area B), and Nanhui New Town (Area C), respectively.

flats in our study (for instance, portions of Areas C and B between 33° 00′00″ and 33° 10′00″). This is one of the factors that contribute to Zhang_TF's large results in Jiangsu Province compared with this study.

5. Conclusion

Using the GEE platform and Sentinel-2 Sensor data, we obtained the tidal flat maps of Jiangsu Province and Shanghai City by the MSIC-Otsu method. The MSIC method was used to obtain the extreme value of the same position on massive images pixel-by-pixel and a composite image of the maximum and minimum water areas, and then the Otsu method was used to identify the tidal flat. The reliability of the MSIC-Otsu extraction was verified for Shanghai City and Jiangsu Province on the basis of time-series Sentinel-2 Sensor acquired images and tide station data. Additionally, the reliability of the results of extracting the boundary lines of the highest and lowest tides was discussed by combining the tide station and image data. The effect of human activity on tidal flats and the irrationality of using the percentile tidal flat extraction method were revealed.

From the confusion matrix of recognition results, the accuracies of users and products of beach are 96.4 and 95.8% respectively. In addition, combining with the real image data, the results of this study are compared with the existing products Murray_TF and Zhang_TF. The results show that the tidal flat data provided by this study in 2021 has high accuracy. This 10-m-resolution map of tidal flats in Shanghai City and Jiangsu Province for 2021 serves as reference for the ecosystem management and sustainable development of tidal flats. Although the method used in this study is mainly aimed at Jiangsu Province and Shanghai City in the Yangtze River Delta region, it can be potentially applied at the spatial scale of larger regions.

Acknowledgments

We thank the Google Earth Engine platform and the European Space Agency for providing free access to the Sentinel-2 Sensor datasets. We also thank the National Oceanographic Science Data Center for tidal station tide height data and the anonymous reviewers and editors for their constructive suggestions. This research was supported by the National Natural Science Foundation of China (grant no. 42371441), the Shanghai Ocean Bureau Research Project (grant no. Shanghai 2023-01), and the Science and Technology Innovation Fund Project of Hydrology Bureau of Yangtze River Water Resources Commission (grant no. SWJ-CJX23 Z06).

References

1 X. Liu, Z. Gao, J. Ning, and Q. Lu: SPIE Digital Library (2014). https://doi.org/10.1117/12.2058414
2 X. Liu, Z. Gao, J. Ning, X. Yu, and Y. Zhang: IEEE J. Sel. Top. Appl. Earth Obs. Remote Sens. **9** (2016) 5123. https://doi.org/10.1109/JSTARS.2016.2616514
3 X.-B. Liu, J. R. Haney, G. Cantero, J. R. Lambert, M. Otero-Garcia, B. Truong, A. Gropman, I. Cobos, S. D. Cederbaum, and G. S. Lipshutz: JCI Insight **4** (2019) 130260. https://doi.org/10.1172/jci.insight.130260
4 N. J. Murray, Z. Ma, and R. A. Fuller: Austral Ecol. **40** (2015) 472. https://doi.org/10.1111/aec.12211
5 Y. Duan, B. Tian, X. Li, D. Liu, D. Sengupta, Y. Wang, and Y. Peng: Int. J. Appl. Earth Obs. Geoinf. **102** (2021) 102383. https://doi.org/10.1016/j.jag.2021.102383

6 M. Wang, D. Mao, X. Xiao, K. Song, M. Jia, C. Ren, and Z. Wang: Remote Sens. Environ. **284** (2023). https://doi.org/10.1016/j.rse.2022.113347
7 M. Schuerch, T. Spencer, S. Temmerman, M. L. Kirwan, C. Wolff, D. Lincke, C. J. McOwen, M. D. Pickering, R. Reef, A. T. Vafeidis, J. Hinkel, R. J. Nicholls, and S. Brown: Nature **561** (2018) 231. https://doi.org/10.1038/s41586-018-0476-5
8 J. MacKinnon, Y. I. Verkuil, and N. Murray: Occasional paper of the IUCN species survival commission, (2012) 47.
9 M. Jia, Z. Wang, D. Mao, C. Ren, C. Wang, and Y. Wang: Remote Sens. Environ. **255** (2021) 112285. https://doi.org/10.1016/j.rse.2021.112285
10 X. Li, X. Zhang, C. Qiu, Y. Duan, S. Liu, D. Chen, L. Zhang, and C. Zhu: Int. J. Environ. Res. Public Health **17** (2020) 1636. https://doi.org/10.3390/ijerph17051636
11 J. Xiao, Z. Ma, and T. Ding: Waste Manage. (Oxford) **48** (2016) 334. https://doi.org/10.1016/j.wasman.2015.09.018
12 D. Sengupta, R. Chen, M. Meadows, Y. R. Choi, A. Banerjee, and Z. Xia: Remote Sens. **11** (2019) 2621. https://doi.org/10.3390/rs11222621
13 X. Hou, T. Wu, W. Hou, Q. Chen, Y. Wang, and L. Yu: Sci. China Earth Sci. **59** (2016) 1791. https://doi.org/10.1007/s11430-016-5317-5
14 H. Li, M. Jia, R. Zhang, Y. Ren, and X. Wen: Remote Sens. **11** (2019) 2479. https://doi.org/10.3390/rs11212479
15 X. Liu, Z. Shao, G. Cheng, S. Lu, Z. Gu, H. Zhu, H. Shen, J. Wang, and X. Chen: Rev. Aquacult. **13** (2021) 1060. https://doi.org/10.1111/raq.12512
16 C. Ren, Z. Wang, Y. Zhang, B. Zhang, L. Chen, Y. Xi, X. Xiao, R. B. Doughty, M. Liu, M. Jia, D. Mao, and K. Song: Int. J. Appl. Earth Obs. Geoinf. **82** (2019) 101902. https://doi.org/10.1016/j.jag.2019.101902
17 K. Tan, J. Chen, W. Zhang, K. Liu, P. Tao, and X. Cheng: ISPRS J. Photogramm. Remote Sens. **159** (2020) 129. https://doi.org/10.1016/j.isprsjprs.2019.11.003
18 N. J. Murray, S. R. Phinn, M. DeWitt, R. Ferrari, R. Johnston, M. B. Lyons, N. Clinton, D. Thau, and R. A. Fuller: Nature **565** (2019) 7738. https://doi.org/10.1038/s41586-018-0805-8
19 M. Chang, P. Li, Z. Li, and H. Wang: Remote Sens. **14** (2022) 1789. https://doi.org/10.3390/rs14081789
20 S. Sagar, D. Roberts, B. Bala, and L. Lymburner: Remote Sens. Environ. **195** (2017) 153. https://doi.org/10.1016/j.rse.2017.04.009
21 X. Wang, X. Xiao, Z. Zou, L. Hou, Y. Qin, J. Dong, B. Doughty R, B. Chen, X. Zhang, Y. Chen, J. Ma, B. Zhao, and B. Li: ISPRS J. Photogramm. Remote Sens. **163** (2020) 312. https://doi.org/10.1016/j.isprsjprs.2020.03.014
22 N. Murray, S. Phinn, R. Clemens, C. Roelfsema, and R. Fuller: Remote Sens. **4** (2012) 3417. https://doi.org/10.3390/rs4113417
23 K. Zhang, X. Dong, Z. Liu, W. Gao, Z. Hu, and G. Wu: Remote Sens. **11** (2019) 924. https://doi.org/10.3390/rs11080924
24 R. Xu, S. Zhao, and Y. Ke: IEEE J. Sel. Top. Appl. Earth Obs. Remote Sens. **14** (2021) 190. https://doi.org/10.1109/JSTARS.2020.3038648
25 Y.-S. Xu, L. Ma, Y.-J. Du, and S.-L. Shen: Nat. Hazard. **63** (2012) 1255. https://doi.org/10.1007/s11069-012-0220-7
26 Q. Wang, W. Shi, Z. Li, and P. M. Atkinson: Remote Sens. Environ. **187** (2016) 241. https://doi.org/10.1016/j.rse.2016.10.030
27 Z. Zhu and C. E. Woodcock: Remote Sens. Environ. **118** (2012) 83. https://doi.org/10.1016/j.rse.2011.10.028
28 R. Zhang, M. Jia, Z. Wang, Y. Zhou, D. Mao, C. Ren, C. Zhao, and X. Liu: Int. J. Appl. Earth Obs. Geoinf. **112** (2022) 102918. https://doi.org/10.1016/j.jag.2022.102918
29 H. Xu: Int. J. Remote Sens. **27** (2006) 3025. https://doi.org/10.1080/01431160600589179
30 C. J. Tucker: Remote Sens. Environ. **8** (1979) 127. https://doi.org/10.1016/0034-4257(79)90013-0
31 W. Cao, Y. Zhou, R. Li, and X. Li: Remote Sens. Environ. **239** (2020). https://doi.org/10.1016/j.rse.2020.111665
32 A. K. Bhandari, I. V. Kumar, and K. Srinivas: IEEE Trans. Instrum. Meas. **69** (2020) 1871. https://doi.org/10.1109/TIM.2019.2922516
33 C. Fan, K. Ren, Y. Zhang, and L. Yi: J. Cent. South Univ. **23** (2016) 880. https://doi.org/10.1007/s11771-016-3135-8
34 Z. Zhang, N. Xu, Y. Li, and Y. Li: Remote Sens. Environ. **269** (2022) 112799. https://doi.org/10.1016/j.rse.2021.112799
35 Y. Chen, J. Dong, X. Xiao, M. Zhang, B. Tian, Y. Zhou, B. Li, and Z. Ma: Sci. Rep. **6** (2016) 1. https://doi.org/10.1038/srep24018
36 C. Zhao, C.-Z. Qin, and J. Teng: ISPRS J. Photogramm. Remote Sens. **159** (2020) 256. https://doi.org/10.1016/j.isprsjprs.2019.11.022

About the Authors

Kuifeng Luan received his B.S. degree from Liaoning Technical University, China, in 2004 and his Ph.D. degree from Tongji University, China, in 2017. From 2015 to 2019, he was a lecturer at Shanghai Ocean University, China. Since 2019, he has been an associate professor at Shanghai Ocean University, China. His research interests are in ocean observation based on satellite and LiDAR data quality control. (kfluan@shou.edu.cn)

Haixia Wan received her Bachelor's degree from Anhui Normal University, China in 2021. She is currently a master's student at the School of Marine Science and Ecology, Shanghai Ocean University, China. Her research interest is in ocean remote sensing. (m210200598@st.shou.edu.cn)